Fuel 358 (2024) 130175

Contents lists available at ScienceDirect

Fuel

journal homepage: www.elsevier.com/locate/fuel

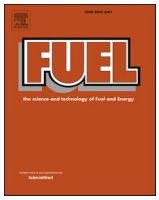

Full Length Article

Investigation on laminar burning velocity measurements of premixed Ethane-Air mixture at higher pressure and temperature conditions

Vijay Shinde [a,*], Amardeep Fulzele [a], Sudarshan Kumar [a]

[a] Department of Aerospace Engineering, Indian Institute of Technology Bombay, Powai, Mumbai 400076, India

ARTICLE INFO

Keywords:
Ethane-air flames
Laminar burning velocity
Pressure exponent
Temperature exponent
Engine relevant conditions

ABSTRACT

The externally heated diverging channel (EHDC) method was utilized to evaluate the laminar burning velocity (LBV) of premixed ethane-air flames at higher mixture temperature (350-620 K) and pressure (1-5 atm) conditions over different mixture strengths (ϕ = 0.7-1.3). The maximum LBV was noted at ϕ = 1.1 for all pressure and temperature conditions. The inverted parabolic behavior of the temperature exponent was obtained with the minima at ϕ = 1.1. The pressure exponent (β) exhibits a parabolic variation with its maxima at ϕ = 1.0. The current results are further analyzed and compared with the literature measurements, and the comprehensive kinetic model predictions of USC mech II, San Diego mech, and Aramco mech 1.3. The present LBV measurements match well with the kinetic model predictions of Aramco mech 1.3 at most of the mixture and pressure conditions. The present results propose the variation of pressure exponent (β) as a function of temperature ratio, and temperature exponent (α) as a function of pressure ratio for different mixture conditions (ϕ). A revised power-law correlation for α and β variations is also recommended as, $S_u = S_{u0}(T_u/T_{u0})^{\alpha_0 + \alpha_1(1 - P_u/P_{u0}))}(P_u/P_{u0})^{\beta_0 + \beta_1(1 - T_u/T_{u0})}$. The sensitivity analysis indicates the maximum decrement in the positive sensitivity for the chain branching reaction HCO + M ↔ H + CO + M (R30) across all the stated mixture conditions, owing to an increment in the third body effects along with pressure and temperature. The reaction pathway analysis reveals a maximum net reduction in the elemental flux (~56 %) for the reaction between the species carbon monoxide (CO) and carbon dioxide (CO_2) through different reactions, due to a rise in pressure and temperature.

1. Introduction

Due to strict emission norms for reducing the greenhouse gas emissions released from the combustion of hydrocarbon fuels, the combustion community has been aggressively working on the goal of reducing the same through the application of alternate fuels with high hydrogen content, such as natural gas and ethane gas. The combustion of natural gas and ethane produces relatively lower CO_2 emissions than commercial gasoline and/or diesel fuels due to its simple chemical structure, relatively higher hydrogen content, complete mixing, and no fuel atomization, spray, mixing, and evaporation issues. The high-octane number of these fuels allows the engine to operate at a high compression ratio, with better anti knocking capability, leading to further improvement of engine power output, thermal efficiency and thereby improved performance.

Ethane has a high heating value (47.2 MJ/kg) as compared to gasoline (44 MJ/kg), which leads to higher flame temperatures and higher combustion efficiency. In general, the benefits of employing ethane in combustors over other fossil fuels include cleaner burning, higher efficiency, adaptability, accessibility and storage, and affordability. Before using ethane as an alternative to fossil fuel in present-day combustors, fundamental combustion investigations should be performed, such as extinction limits, laminar burning velocity (LBV), and ignition time studies. The LBV is an important parameter that specifies the speed at which a flame front propagates through a combustible mixture. At higher temperatures and pressures, such as those observed in gas turbine combustors and internal combustion engines, the LBV of a fuel-air mixture can have a major influence on emissions, combustion process, and combustion efficiency. As a result, a thorough understanding of the LBV of the ethane-air mixture under higher pressure and temperature conditions is critical for refining the combustion system design, lowering the combustion emissions, boosting efficiency, and assuring safe operation at all operating conditions.

In the past, various experimental and computational studies have

* Corresponding author.
E-mail address: vijay150976@gmail.com (V. Shinde).

https://doi.org/10.1016/j.fuel.2023.130175
Received 22 July 2023; Received in revised form 7 October 2023; Accepted 23 October 2023

Table 1
Summary of LBV measurement of ethane-air mixtures at different conditions (1990 onwards). SEF - Spherically expanding flame, EHDC - Externally heated diverging channel, SF - Stagnation flame, HF - Heat flux, BF - Bunsen flame.

Ref.	Method	Operating conditions		
		P_u (atm)	T_u (K)	ϕ
Egolfopoulos (1990) [2]	SF	0.25-3	298	0.6-2
Aung (1995) [5]	SEF	1	298	0.8-1.6
Vagelopoulos (1998) [15]	SF	1	298	0.7-1.4
Hassan (1998) [1]	SEF	0.5-4	298	0.8-1.6
Konnov (2003) [3]	HF	1	353	0.6-1.6
Bosschart (2004) [16]	HF	1	298	0.6-1.5
Jomaas (2005) [6]	SF	1-5	298	0.7-1.4
Dyakov (2007) [17]	HF	1	298	0.6-1.5
Kishore (2008) [7]	HF	1	307	0.7-1.3
Lowry (2010) [8]	SEF	1-10	298	0.7-1.3
Dirrenberger (2011) [18]	HF	1	298	0.6-2.1
Park (2013) [19]	SF	1	298	0.6-1.5
Mitu (2014, 2015) [9,10]	SEF	0.3-1.3	298-433	0.6-1.3
Goswami (2016) [11]	HF	1-4	298	0.8-1.3
Han (2019) [12]	HF	1	298-328	0.7-1.5
Ghosh (2022) [20]	BF	1	180-295	0.8-1.4
Shinde (2023) [13]	EHDC	1	350-660	0.7-1.3

been reported to evaluate the LBV of the C_2H_6-air mixture at higher pressure and temperature conditions. Different measurement methods have been used to estimate the LBV, such as the spherical bomb method [1], counterflow flame method [2], and heat-flux method [3]. Amidst these techniques, the heat-flux method solely measures the stretch-free LBV at adiabatic conditions, which is also considered as direct method for the estimation of LBV.

Egolfopoulos et al. [2] used the stagnation flame method to evaluate the burning velocity of C_2H_6-air mixtures (ϕ = 0.6 to 2.0) at pressures (0.25-3 atm) and normal temperature conditions. They discussed the comparative importance of individual reactions on the LBV using sensitivity analysis. At normal temperatures, the measured burning velocity was reduced by 45 %, as the pressure rises from 0.25 to 3 atm. Tseng et al. [4] employed the spherically expanding flame method (ϕ = 0.8-1.6) at normal conditions to analyze the influence of flame stretch on the burning velocity of C_1-C_3 alkane fuels. At reference conditions, they observed a maximum burning velocity of 44 cm/s (ϕ = 1.1) for the C_2H_6-air mixture. Due to the variation in the heat of formation, which altered the density ratios under similar conditions, Aung et al. [5] rectified the burning velocity presented by Tseng et al. [4] and revised the maximum burning velocity to 37 cm/s. Hassan et al. [1] determined the LBV utilizing the spherical bomb method (ϕ = 0.8-1.6) at standard temperature and pressures (0.5-4 atm). With an increase in pressure, they observed negative Markstein numbers for the wider mixture ranges, which led to various flame instabilities due to preferential diffusion at high-pressure conditions. Jomaas et al. [6] employed the spherical bomb method to evaluate the LBV (ϕ = 0.7-1.4) at normal temperature, and pressures (1, 2, and 5 atm). The adiabatic LBV of C_2H_6-air mixtures (ϕ = 0.7-1.3) are measured by Kishore et al. [7] utilizing the heat flux method at 1 bar and 307 K. They observed maximum LBV (41 cm/s, ϕ = 1.1) at standard conditions. Identifying the significance of natural gas as a vital fuel in industrial gas turbines for power generation, Lowry et al. [8] used the stagnation flame method to evaluate the burning velocity of C_2H_6-air mixtures (ϕ = 0.6-1.3) at different pressures (1, 5 and 10 atm) and standard temperatures. They developed a hybrid correlation to estimate the uncertainties through a meticulous analysis. Mitu et al. [9,10] estimated the burning velocity (ϕ = 0.59-1.36) utilizing the spherically expanding flame method at pressures (P_u = 30-130 kPa) and temperatures (T_u = 298-433 K). They also presented temperature and pressure coefficients using the power-law correlations. In 2016, Goswami et al. [11] used the heat-flux method to evaluate the burning velocity (ϕ = 0.8-1.3) at pressures (P_u = 1-4 atm) and normal temperature conditions. They observed significant deviation in the measured pressure exponent values as compared to the mechanism predictions and literature results. Han and co-workers [12] employed the heat-flux method to determine the burning velocity of C_2H_6-air mixture for different mixture ranges (ϕ = 0.7-1.5) at different mixture temperatures (T_u = 298-328 K) and standard pressure conditions. They suggested a temperature exponent correlation to indicate the temperature dependency on the burning velocity. Recently Shinde et al. [13] determined the LBV of C_1-C_4 alkane-air mixtures (ϕ = 0.7-1.3) utilizing the diverging channel method at elevated temperature (350-660 K) and standard pressure conditions. From the power-law correlation, they also deduced the temperature exponents for the stated mixture strengths (ϕ), to indicate the temperature dependency of the LBV. The LBV data at higher pressures and temperatures are beneficial for improving/validating various kinetic models of different fuels. This data further helps in combustion modeling of gas turbine combustors, industrial furnaces and internal combustion engines.

The LBV of a fuel-air mixture depends upon the mixture strength (ϕ), unburnt mixture temperature (T_u), and pressure (P_u). The long-term measurements are presented as a power-law correlation between the mixture temperature and pressure, as shown below [14].

$$S_u = S_{u0}\left(\frac{T_u}{T_{u0}}\right)^{\alpha}\left(\frac{P_u}{P_{u0}}\right)^{\beta} \quad (1)$$

where P_{u0} and T_{u0} are standard pressure and temperature (1 atm and 300 K), respectively. S_{u0} is the LBV at (P_{u0}, T_{u0}), and S_u is the LBV at pressure P_u and temperature T_u. The α and β are temperature and pressure exponents, respectively.

A detailed review of the existing literature on the measurement of premixed ethane-air flames at different conditions is summarized from 1990 onwards in Table 1. It is clear from Table 1 that although several experimental studies have been reported at standard pressure and temperature conditions, there are very limited studies at elevated pressure and temperature conditions. There is only one study by Mitu et al. [9,10], which reports the simultaneous effect of elevated pressure (0.3-1.3 bar) and temperatures (298-433 K) using the spherical expanding flame method. To our knowledge, there are no other studies that report the simultaneous effect of elevated pressure (1-5 atm) and temperature (350-620 K) on the variation of LBV of ethane-air mixtures.

Fig. 1 shows the comparison of present experimental operating conditions with the available literature data as listed in Table 1, along with the thermodynamic conditions encountered in a typical engine during the mixture compression process. In Fig. 1, lines I and II imitate the isentropic compression process following, $T_u/T_{uo} = (P_u/P_{uo})^{(\gamma-1)/\gamma}$, where T_{u0} and P_{u0} are initial temperature and pressure respectively, and γ is the specific heat capacity ratio of the unburned gas. Region 1 between lines I and II represents the typical T_u and P_u range expected during the compression and combustion processes in spark ignition (SI) engines, and these conditions are considered as engine relevant conditions. Most of the previously reported studies are along lines III and IV shown in Fig. 1, and they are referred to as unrealistic engine conditions because they are far away from region 1. The present study is an attempt towards the measurement of the laminar burning velocity in this direction and reports the LBV values near the engine relevant conditions, (area highlighted with yellow color in Fig. 1). Similar studies at engine relevant conditions for methane-air mixtures were reported by Varghese et al. [21] and propane-air mixtures by Shinde et al. [22] using EHDC method recently.

The pressure exponents (β) are observed at standard temperature, and temperature exponents (α) are noted at 1 atm pressure conditions by all investigators. Individually, pressure and temperature exponents are presumed to be constant at high temperatures and pressure conditions, respectively. The comprehensive LBV measurements performed simultaneously at elevated temperature and pressure conditions would help provide an improved understanding of the influence of mixture temperature on β and mixture pressure on α.

The EHDC method is utilized in this investigation to determine the

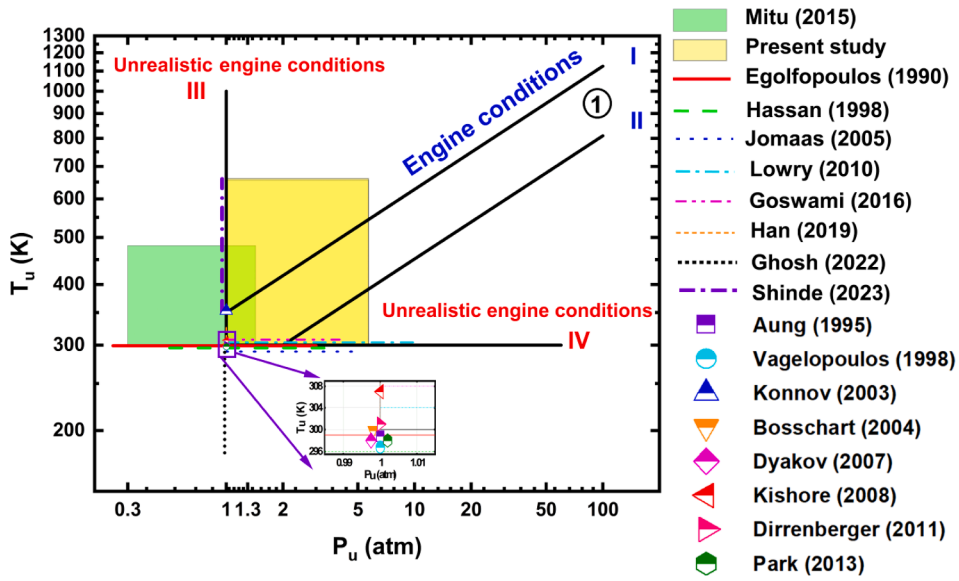

Fig. 1. Summary of the experimental conditions for the LBV measurement in the present work and its comparison with the available literature data as listed in Table 1 and engine relevant conditions.

LBV variation for C_2H_6-air mixtures at higher pressure and temperature conditions simultaneously. The current measurements are conducted at higher mixture temperature (350-620 K) and pressure (1-5 atm) conditions. The temperature and pressure exponents of the ethane-air mixtures are evaluated from the power-law correlations. The mechanism predictions utilizing three comprehensive reaction mechanisms (Aramco mech 1.3 [23], USC mech II [24], and San Diego mech [25]) are compared with the literature and current results. The reduction in the mixture LBV with a rise in mixture pressure is thoroughly studied. The pressure and temperature exponents from the current work are analyzed with the mechanism predictions and literature data. Lastly, a revised power-law correlation for the burning velocity estimation is presented, indicating the dependency of β on the temperature ratio and α on the pressure ratio. The influence of chemical kinetics on the LBV are also discussed with the help of sensitivity and reaction pathway diagrams.

2. Experimental and modeling details

2.1. Experimental setup

A 10° diverging channel made of quartz glass is utilized in the present investigation to get the planar stabilized flames for determining the burning velocities. The experimental setup details are similar to earlier

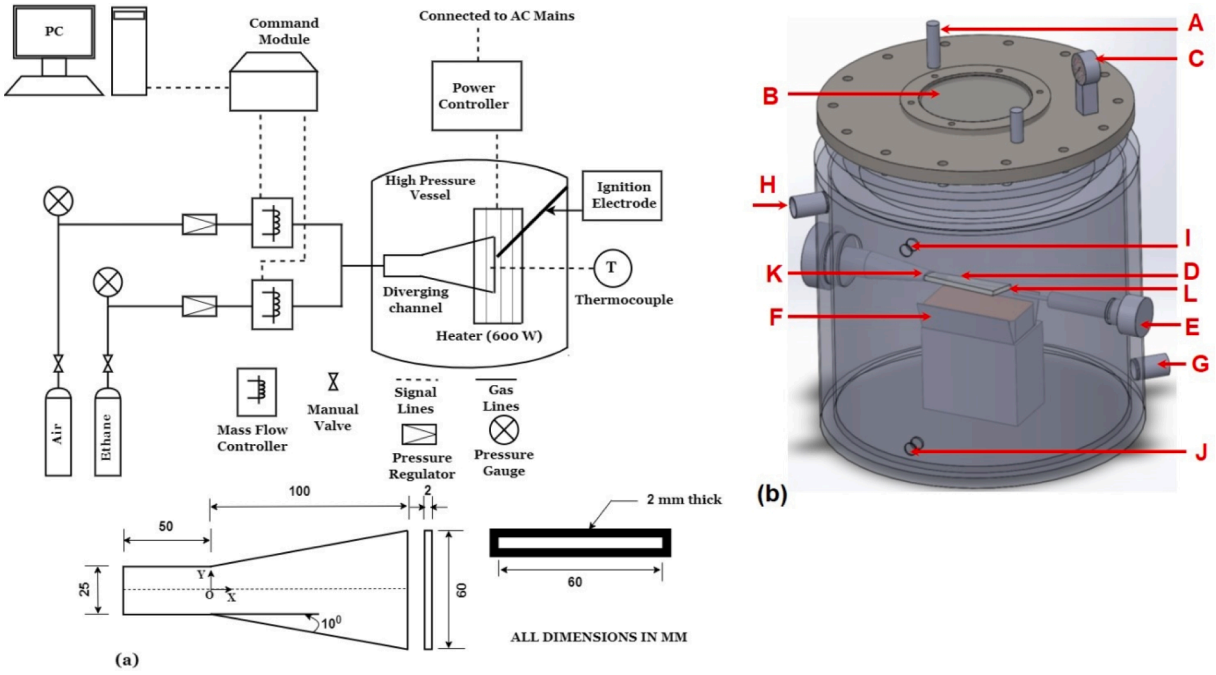

Fig. 2. (a) Layout of the experimental setup, (b) Stainless steel cylindrical pressure vessel; A - Pressure relief valve, B - Quartz glass window, C - Pressure gauge, D - Diverging channel, E - Thermocouple, F - Ceramic heater, G - Cooling water inlet, H - Cooling water outlet, I, J - Pressurizing Air inlet, K - Fuel-air mixture inlet, L - Exhaust gas outlet.

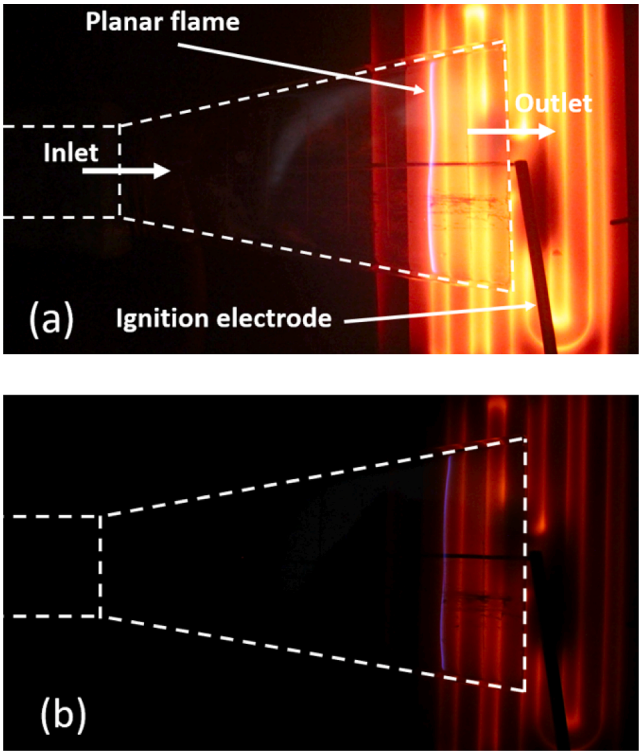

Fig. 3. Direct photograph of a planar stabilized flame at (a) $\phi = 0.8$ with $U_{in} = 0.9$ m/s at 2 atm, 563 K and (b) $\phi = 1.0$ with $U_{in} = 1.05$ m/s at 5 atm, 604 K.

work [21]. A ceramic heater (600 W) is employed to heat the diverging channel externally. A positive temperature gradient develops along the length of the channel due to external heating. A high aspect ratio (12.5) of the channel provides uniform velocity and temperature profiles along the transverse direction of the channel [26]. This helps to get the stable planar flames within the channel. The heat loss from the reaction zone to the channel walls is compensated by the external heat of the heater, which assists in achieving close to adiabatic conditions at the flame location [26]. The diverging channel and heater are placed in a stainless steel cylindrical pressure vessel (40 L), as indicated in Fig. 2. The ceramic heater is kept 20 mm below the diverging channel. The pressure regulation within the vessel is achieved by the pressure relief valve. The premixed fuel-air mixture at the desired velocity and mixture condition (ϕ) is fed to the channel. An ignition device is kept at the outlet plane of the channel to ignite the premixed fuel-air mixture within the channel. After the mixture ignition, the flame progressively travels in the upstream direction and stabilizes at a location where the mixture LBV matches the local flow velocity. The unburnt mixture temperature and the flame cross-section area at the location of the stabilized flame are determined to estimate the mixture LBV through the application of the mass conservation equation. This process is repeated for various mixture conditions and different heat inputs. As the flow Peclet number within the diverging channels (width 2 mm) is low, the unburnt mixture temperature is considered to be close to the inner channel wall temperature at the stabilized flame position [27,28]. The direct photographs of a stabilized planar flame are presented in Fig. 3 at different operating conditions.

2.2. Temperature measurement and distribution

The LBV measurement using the EHDC method relies on unburnt mixture temperature data and flame location. In the beginning, a K-type thermocouple is employed to determine the air temperature within the channel at different axial positions under cold flow conditions at various flow rates [21]. An accurate traverse mechanism is utilized to operate the thermocouple throughout the length of the channel. The thermocouple records the temperature of the lower channel wall. The temperature distribution across the channel is determined a priori for various external heating rates at different flow rate conditions. Fig. 4 depicts the temperature distribution across the channel (cold flow conditions) for an external heating rate (400 W) and an inlet velocity of $U_{in} = 1$ m/s. Fig. 4b demonstrates almost constant temperature in the transverse direction with a maximum deviation of $\pm$ 3 K. This uniform temperature distribution assists in obtaining planar flames over a wide range of mixture velocities and equivalence ratios (ϕ). A linear positive temperature gradient of 5.05 K/mm was noted along the mixture flow direction at the stated conditions. Fig. 4a illustrates that at a given heating rate (400 W), the temperature and temperature gradient at 2 atm pressure (5.05 K/mm) is lower than at 1 atm pressure (6.17 K/mm) because the unburnt mixture temperature reduces as the pressure increases. Therefore, higher heating rates are required from the external heater at high-pressure conditions.

2.3. Evaluation of mixture LBV

The LBV is measured in the EHDC method at the position of the planar stabilized flame, where the LBV matches the inlet mixture velocity. The position of the stabilized planar flame depends upon the mixture condition (ϕ), external heat input, and inlet mixture velocity. The LBV (S_u) is estimated utilizing a rearranged mass conservation equation as follows:

$$S_u = U_{inlet} \times \left(\frac{A_{inlet}}{A_f}\right)\left(\frac{T_u}{T_{in}}\right) \quad (2)$$

where A_{inlet} and U_{inlet} represent the cross-section area at the inlet of the channel (m^2) and inlet mixture velocity (m/s), respectively, T_u and A_f indicate the unburnt mixture temperature and channel cross-section area at the stabilized flame location, and T_{in} indicate the unburnt mixture temperature at the inlet of channel.

2.4. Uncertainty estimation

The error propagation rule is utilized to estimate the uncertainty for the present measurements [26,29]. The mixture temperature, inlet velocity, and flame area all influence the uncertainty of the estimated LBV [26]. The uncertainty of the mass flow controllers (AALBORG® GFC17) utilized for air and fuel measurement ranges up to 1.5 % of the full-scale reading. The K-type thermocouple utilized has a standard uncertainty of $\pm$ 2.2 K or 0.75 % of reading, whichever is maximum. The traverse mechanism used to move the thermocouple within the diverging channel has a $\pm$ 1 mm precision, resulting in a $\pm$ 0.71 mm^2 uncertainty in the flame area calculation [30]. At higher mixture pressure and temperature conditions, the highest uncertainty recorded for the estimated LBV is found to be less than $\pm$ 5 % [21]. The least squares method recommended by Alekseev et al. [31] was employed to estimate the uncertainty in the pressure exponent (β) and temperature exponent (α). The highest temperature and pressure exponent uncertainty was estimated to be $\Delta\alpha = 0.1212$ and $\Delta\beta = 0.059$, respectively. The supplementary material comprises brief descriptions of the estimation of various uncertainties in the present measurements.

2.5. Numerical modeling details

The CHEMKIN-Pro 2020 [32] software package was utilized for computational studies to estimate the LBV using different detailed reaction mechanisms (Aramco mech 1.3 [23], USC mech II [24], and San Diego mech [25]). The mixture-averaged transport property condition is employed to compute the transport properties of a 1-D adiabatic laminar flame. The grid convergence is confirmed by using adaptive mesh

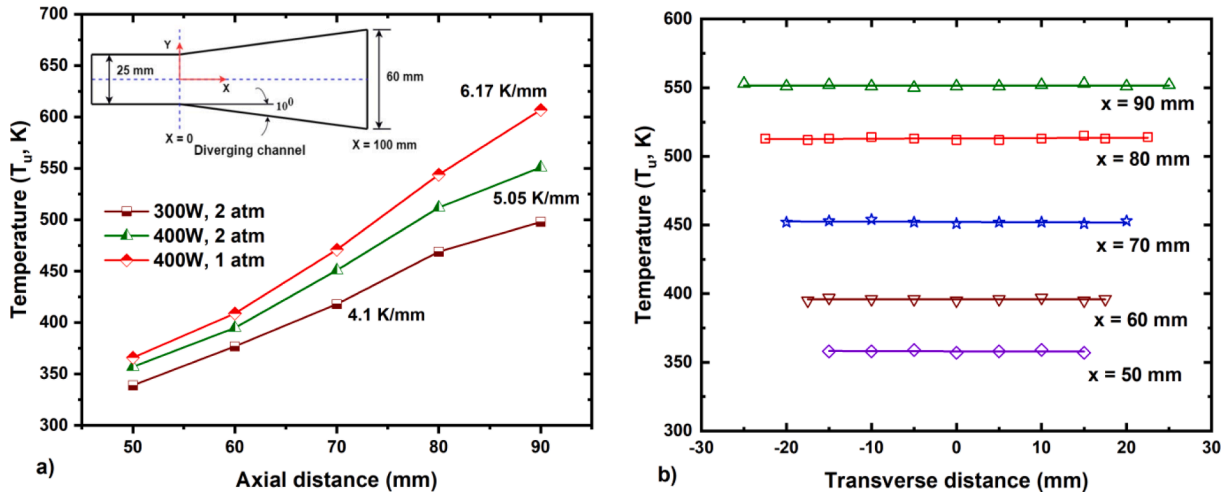

Fig. 4. (a) Temperature distribution in the axial direction for different heating rates (U_{in} = 1 m/s, P_u = 1, 2 atm). (b) Temperature distribution in the transverse direction (Q = 400 W, U_{in} = 1 m/s, P_u = 2 atm).

parameters CURV (0.03), GRAD (0.04), and a maximum of 2000 grid points to discretize over the length of the domain.

3. Results and discussion

3.1. Influence of higher mixture temperature on LBV (P_u = 2 atm)

Fig. 5 depicts the LBV (S_u) variation with temperature ratio (T_u/T_{u0}) for ethane-air mixtures. The lines depict the different mechanism predictions, and symbols indicate the experimental data. The power-law correlations, $S_u = S_{u0} \times (T_u/T_{u0})^{\alpha}$ was used to plot the measured data, where T_u is the unburnt mixture temperature, T_{u0} is the standard reference temperature (300 K), S_{u0} is the LBV at 300 K temperature, and α is the temperature exponent. The plot clearly depicts that the burning velocity enhances with an increase in the unburnt mixture temperature, owing to the elevated adiabatic flame temperature and enthalpy content of the fuel-air mixture. The differences in the kinetic variables (viz. reaction rate constants, third body efficiencies, and reaction activation energies), the exclusion or inclusion of various reactions in these extensive kinetic models, and certain species in these reaction mechanisms primarily affect the LBV variation at different conditions. Fig. 5 depicts that for stoichiometric mixture condition, the present results are

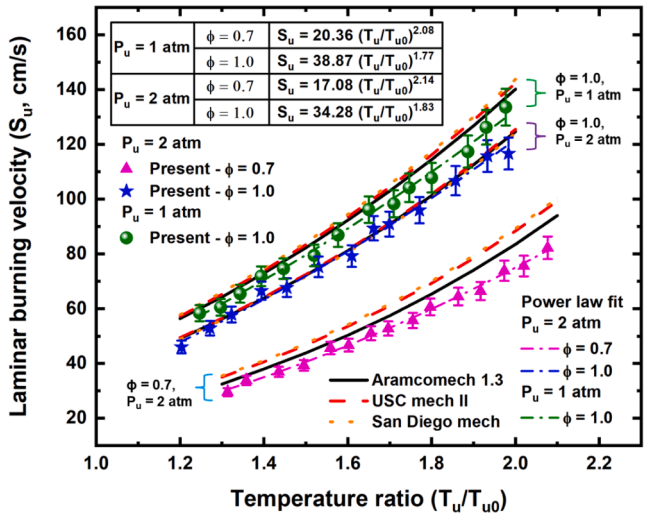

Fig. 5. Variation of LBV for the ethane-air mixture at higher temperatures and pressures (P_u = 1, 2 atm) for ϕ = 0.7 and 1.0.

consistent with all three kinetic model predictions across the whole temperature ratio range within the uncertainty limits. At ϕ = 0.7, the present results are somewhat lower than the mechanism predictions; however, they are closer to the mechanism predictions of Aramco mech 1.3 [23]. The inset table illustrates the equation and the power-law fit parameters. Identical equations are obtained for various mixture conditions (ϕ) and high pressures (P_u = 1-5 atm), assisting in the evaluation of burning velocity (S_{u0}) at reference conditions and the corresponding temperature exponent (α) values. As per the current measurements, at ϕ = 1.0, S_{u0} = 34.28 cm/s with a temperature exponent, α = 1.83 value is noted for P_u = 2 atm pressure. At the stoichiometric mixture condition, Fig. 5 indicates a decrement in the LBV owing to the rise in mixture pressure (1 to 2 atm).

3.2. Influence of higher mixture pressures on LBV at 300 K

The power law correlation was employed to extract the LBV data (S_{u0}) at reference condition (300 K) by performing experiments at higher pressures (1-5 atm) and temperatures (350-620 K). Fig. 6a compares the present measurements with the predictions of various reaction mechanisms (Aramco mech 1.3 [23], USC mech II [24], and San Diego mech [25]), as well as previous investigations [1,6,10,11] at 300 K for varying mixture strength (ϕ = 0.7-1.3) at 1, 2, and 4 atm pressures. The present measurements are consistent with the kinetic model predictions of Aramco mech 1.3 [23] for lean to stoichiometric mixtures (except slight under prediction at 1 atm) and slight over prediction for rich mixture conditions. The present findings are a good match with the literature data of Goswami et al. [11] from stoichiometric to rich mixture conditions at 1 atm, within the uncertainty limits. The literature results of Goswami et al. [11] and Jomaas et al. [6] show lower LBV values for the majority of the mixture conditions, whereas, at 4 atm pressure, the present results agree well with Goswami et al. [11] at ϕ = 1.2 and 1.3. The experimental investigations of Mitu et al. [10] are at different mixture equivalence ratios than at standard values i.e. 0.7, 0.8, etc. Therefore, the results of Mitu et al. [10] show a slightly different trend than the existing data in the literature. Fig. 6b depicts a similar comparison of current results at 3 and 5 atm with the mechanism predictions [23–25] and literature results [1,8,11]. In Fig. 6b, different scales on the y-axis (LHS 3 atm, RHS 5 atm) are adopted to prevent overlapping of the data. The present results are in good match with the kinetic model predictions of Aramco mech 1.3 [23] within uncertainty limits, both at 3 and 5 atm pressures. The literature results of Goswami et al. [11] match well at ϕ = 1.2 and 1.3, and show lower LBV values from lean to slightly rich mixture conditions, as compared to the present results at 3 and 5

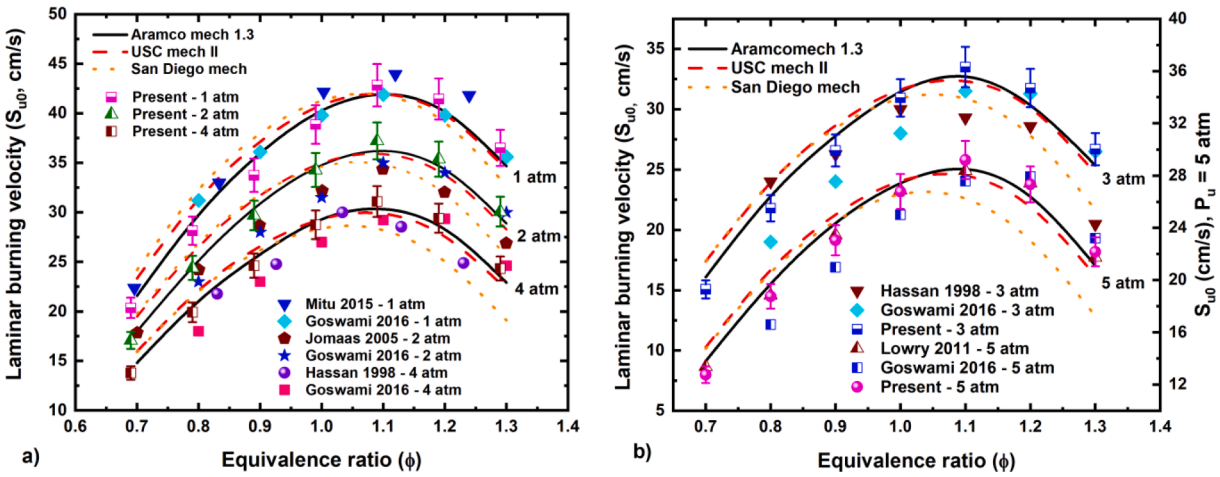

Fig. 6. LBV of the ethane-air mixture at different pressures (a) 1, 2, 4 atm, and (b) 3, 5 atm and reference temperature (300 K) with mechanism predictions (lines) and literature results (symbols).

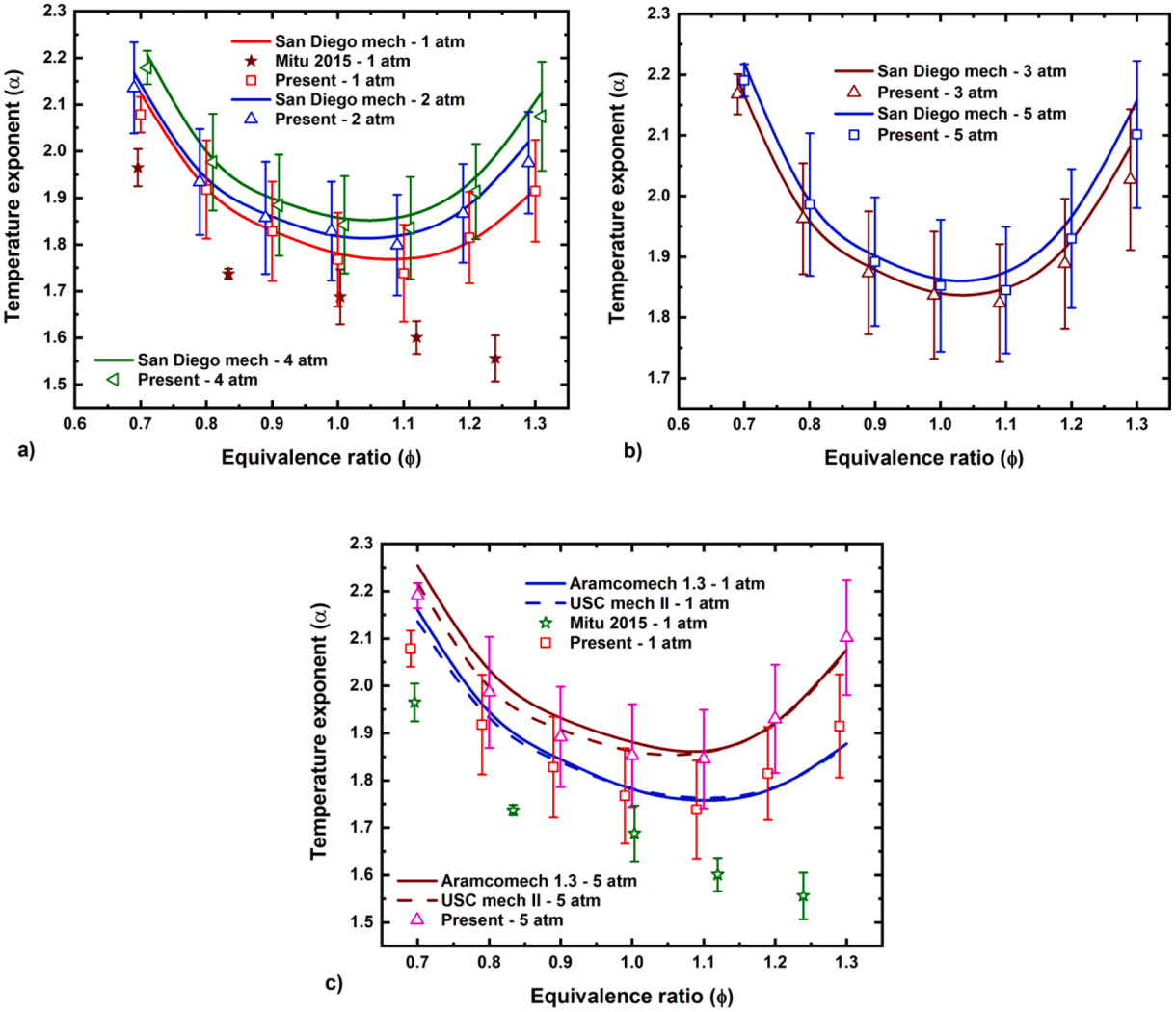

Fig. 7. Variation of temperature exponent (α) for the ethane-air mixture at different pressures (a) P_u = 1, 2, 4 atm and (b) P_u = 3, 5 atm (c) P_u = 1, 5 atm.

atm pressure conditions. Both Fig. 6a and 6b depict a substantial reduction in LBV values owing to enhanced mixture pressure.

The entire mixture pressure dependency of LBV can be expressed in the form,

$$S_u = S_{u0}\left(\frac{P_u}{P_{u0}}\right)^{\beta} \quad (3)$$

where S_{u0} is the LBV at reference condition (P_{u0} = 1 atm) and, β - pressure exponent. The pressure exponent, β, is a function of mixture conditions (ϕ) and the pressure range (1-5 atm). The influence of LBV on pressure can be illustrated using the comprehensive and thermal theories of LBV analysis as, $S_u \propto P^{(n-2)/2}$, where n indicates the overall reaction order. The overall reaction order for major hydrocarbon-air mixtures is stated to be lower than 2 with $S_u < 50$ cm/s, implying that the LBV decreases with increasing mixture pressure [33]. As a consequence, for hydrocarbon-air mixtures, the reported pressure exponent (β), is found to be negative. The burning velocity decreases with a rise in pressure owing to density changes in the mixture. The rise in mixture density causes a decrease in the mean free path, which leads to increased molecular collisions, thus raising the collision frequency. This helps in increased third-body recombination reactions as well as third-body effects. The reaction zone thickness decreases with an increase in mixture pressure. The oxidation rate is further affected at high pressures owing to the increased thermal diffusivity of the mixtures [21].

3.3. Change in temperature exponent at higher pressures

The temperature exponent (α), an empirical parameter that demonstrates a rise in LBV at elevated temperatures, was obtained from power-law correlations for the measured LBV data at different pressure conditions and mixture strength (ϕ = 0.7-1.3). Fig. 7a and 7b illustrate a comparison of the observed temperature exponent values with San Diego mech [25] mechanism predictions at different pressures (P_u = 1-5 atm). To avoid data cluttering and better understanding, the current results are somewhat offset on the x-axis by ± 0.01 (P_u = 1, 2, 3, and 4 atm). The influence of pressure on temperature exponents has been studied and reported. For the entire pressure range (1-5 atm), the temperature exponent demonstrates non-monotonic behavior with mixture conditions, and it is noted to be minimal at ϕ = 1.1. The temperature exponents appear to rise slightly owing to an increase in pressure for the range of mixture strength (ϕ). The temperature exponents acquired from the measurements are closer to the mechanism predictions of San Diego mech [25] within the uncertainty limit. These predictions also match well from lean to stoichiometric mixture conditions over the entire pressure range (P_u = 1-5 atm). The measurements of Mitu et al. [10] were noted to be slightly lesser than the present results for the whole mixture conditions (ϕ) at 1 atm. This may be due to the smaller temperature range (298-423 K) and the lower number of data points observed in their literature. Fig. 7c depicts the comparison of the measured temperature exponent values with the mechanism predictions of Aramco mech 1.3 [23] and USC mech II [24] at P_u = 1 and 5 atm pressures. The present measurements are in better agreement with the kinetic model predictions of USC mech II [24] at 1 atm and except at ϕ = 0.7. The predictions of kinetic models at 5 atm match reasonably well with the present measurements.

The temperature exponent, α, is obtained using the power-law correlation, $S_u = S_{u0}\,(T_u/T_{u0})^{\alpha}$, as this equation resembles the Arrhenius equation, $k = AT^{\beta}\exp(-E_A/R_uT)$. Laminar burning velocity is observed to increase with an increase in the mixture temperature due to an increase in the Arrhenius reaction rate and a rise in the enthalpy of reactants. Maximum LBV is observed for stoichiometric and slightly rich mixtures at ϕ = 1.1. At these mixture conditions, the adiabatic flame temperature is also maximum. Due to the occurrence of the highest flame temperature at ϕ = 1.1, the dissociation reactions start playing a major role, which significantly affects the rate at which mixture burning velocity changes with temperature. Therefore, the values of temperature exponents, α, are observed to be minimum for stoichiometric and slightly rich mixture (ϕ = 1.1) conditions. At extreme conditions of very lean and rich mixtures, the adiabatic flame temperature is comparatively lower. Due to this, the role of dissociation reactions is comparatively low. Hence, the values of the temperature exponents are relatively higher as compared to stoichiometric and slightly rich (ϕ = 1.1) mixtures.

3.4. LBV variation at high pressure and high temperature conditions

The burning velocity variation for a range of pressures (P_u = 1-5 atm), as well as high temperature (T_u = 600 K) conditions for various mixture conditions (ϕ = 0.7-1.3), is presented in Fig. 8. The power-law correlations were employed to obtain the current LBV values at various pressure and mixture conditions using the temperature exponent values (α) acquired earlier. It is evident from Fig. 8a that the current measurements are slightly over-predicted by all three kinetic models for lean to stoichiometric mixture conditions. These kinetic models under predict the LBV values for rich mixture conditions at all pressure conditions. Overall, the kinetic model predictions of Aramco mech 1.3 [23] are comparatively closer to the present results, with a maximum deviation of ~ 12 % at ϕ = 0.7 for 1 atm pressure condition. The data of Mitu et al. [10] are plotted using power law correlation based on S_{u0} and α reported in their literature, and similar observations were made for lean to stoichiometric mixture conditions. Identical observation can be made in Fig. 7b for 5 atm pressure conditions, with a maximum deviation of ~ 13 % at ϕ = 0.7. The experimental LBV data of Mitu et al. [9,10] is relatively lower than the present measurements, as shown in Fig. 8a, due to the lower values of temperature exponent reported by them (see Fig. 7a and 7c). Mitu et al. [9,10] obtained the values of temperature exponent α by considering a smaller temperature range of 298-433 K. Further, the linear variation of α with ϕ for lower hydrocarbon fuels was discouraged by Konnov [34]. The study of Mitu et al. [9,10] used cubic law coefficients for obtaining the burning velocities; however, they do not mention about the effect of Markstein length and Lewis number. The effect of Markstein length and Lewis number is very critical in rich mixture conditions. Perhaps this could be one of the important reasons for LBV deviation at high temperature conditions. In general, an increase in the unburnt mixture temperature enhances the LBV of the fuel-air mixture for all equivalence ratios owing to a rise in enthalpy content and a higher concentration of radicals (O, OH, H, and CH_3) at elevated mixture temperatures. The rise in radical species, along with adiabatic flame temperatures, leads to a rapid rate of heat release. The elevated enthalpy of the unburnt mixture enhances the LBV. The LBV decreases due to a rise in the mixture pressure at a certain mixture condition and unburned gas temperature. The subsequent empirical equation can be expressed to indicate the LBV variation at higher temperatures and pressures for stoichiometric mixture condition.

$$S_u = 38.8\left(\frac{T_u}{T_{u0}}\right)^{\propto}\left(\frac{P_u}{P_{u0}}\right)^{\beta};$$
$$\propto = 1.77 + 0.018\frac{P_u}{P_{u0}};\ \beta = 0.0582\frac{T_u}{T_{u0}} - 0.3035 \quad (4)$$

3.5. Pressure exponent variation with the mixture conditions (ϕ)

The burning velocity decreases due to a rise in the mixture pressure for premixed ethane-air flames. Chemical kinetics plays a key role in lowering the mixture LBV with the mixture pressure. The LBV is affected by the variation in the thermophysical properties of the mixture (higher density, thermal diffusivity) as well as changes in the collision frequency of the third-body reactions. The rise in initial pressure has a secondary influence on the transport and thermodynamic properties of the mixture [21]. The LBV (S_{u0}) variation of ethane-air mixtures at various mixture strengths (ϕ) and its reduction with the rise in pressure is indicated in Fig. 9. The pressure-dependent power-law correlation. $S_u = S_{u0}(P_u/P_{u0})^{\beta}$

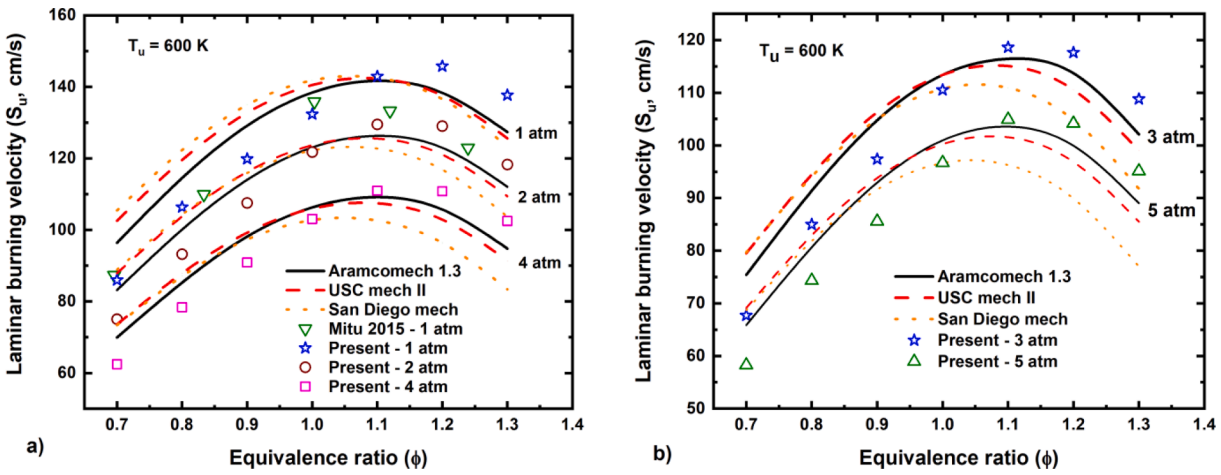

Fig. 8. LBV variation at different pressures [a] P_u = 1, 2, 4 atm and [b] P_u = 3, 5 atm for mixture temperature T_u = 600 K.

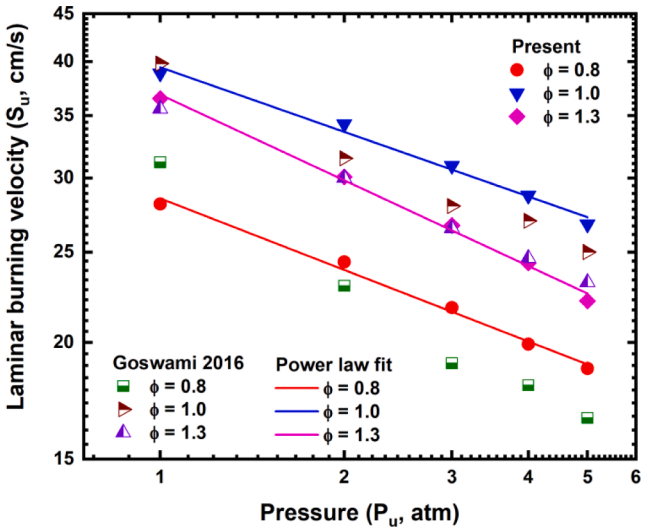

Fig. 9. LBV variation at higher pressures and reference temperature (300 K) of ethane-air mixtures.

is acquired from the slope of these straight lines plotted on the logarithmic scale, as indicated in Fig. 9. The current data are also analyzed with the measurements reported by Goswami et al. [11] at ϕ = 0.8, 1.0, and 1.3. The present experimental measurements are marginally higher than the experimental measurements of Goswami et al. [11], with a maximum deviation of ~ 11 % at ϕ = 0.8 for 5 atm pressure. However, the current measurements agree well with the literature data of Goswami et al. [11] at rich mixture conditions for the entire pressure range.

The pressure exponent values β obtained from Fig. 9 are presented and compared with various mechanism predictions and the literature results in Fig. 10. Fig. 10a depicts the pressure exponent (β) variation with mixture conditions (ϕ) at reference temperature (T_{u0} = 300 K). The pressure exponent (β) values are extracted by applying the power-law correlation to LBV values at 300 K and various pressure conditions. A non-monotonic behavior of pressure exponent (β) was observed with the maximum value at stoichiometric mixture condition. As the number of data points for evaluating pressure exponents is relatively less (at P_u = 1-5 atm), higher uncertainties in β are anticipated in the values reported in the current work (maximum ~ 19 % at ϕ = 0.7). The present measurements agree well with the kinetic model predictions of Aramco mech 1.3 [23] and USC mech II [24] over the entire mixture conditions (ϕ). The pressure exponent values of present measurements are compared with the different literature data [1,6,8,10,11]. For lean mixture conditions, the present results are a good match with the literature data of Lowry et al. [8], whereas for stoichiometric to rich mixture conditions, the present results agree well with the data of Jomaas et al. [6]. A substantial scatter can be noticed in Fig. 10a; this is perhaps owing to various measurements and data extraction techniques used by different investigators. Fig. 10b indicates the pressure exponent

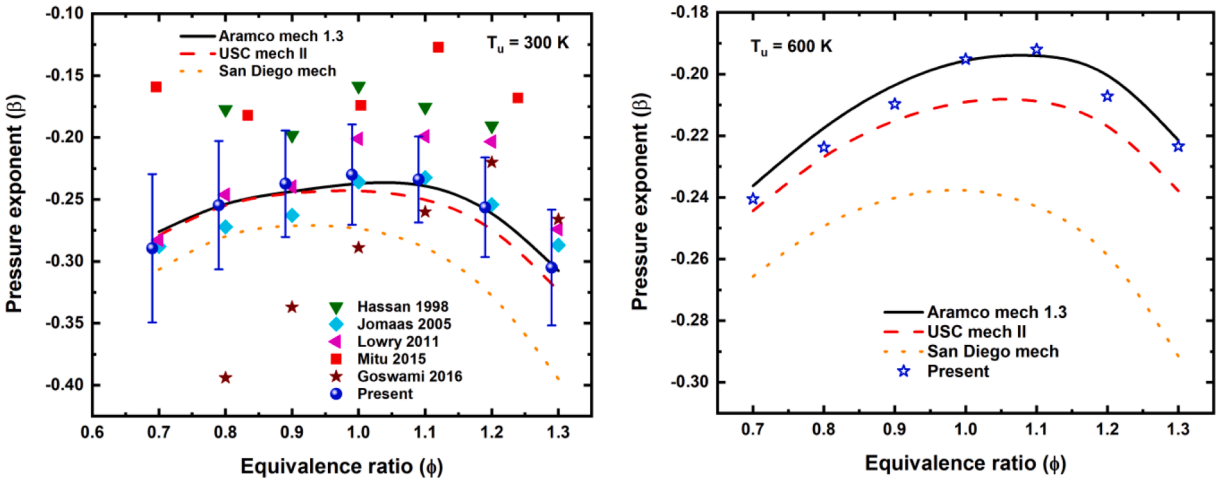

Fig. 10. Pressure exponent variation with the mechanism predictions and literature ([a] T_u = 300 K [b] T_u = 600 K).

(β) variation with mixture conditions (ϕ) at an elevated mixture temperature (T_u = 600 K). The pressure exponent (β) values are obtained by applying the power-law correlation to LBV values at 600 K and various pressure conditions. For lean mixture conditions, the present results are closer to the kinetic model predictions of USC mech II [24], and for stoichiometric to rich mixture conditions, the present results indicate a good match with the kinetic model predictions of Aramco mech 1.3 [23]. Fig. 10b also indicates that substantial deviations exist between the mechanism predictions of San Diego mech [25] and current measurements over the entire range of the mixture conditions (ϕ), suggesting further improvement/modifications in the mechanism.

The values of the pressure exponent, β, are obtained from the power law correlation, $S_u = S_{u0}\,(P_u/P_{u0})^{\beta}$. As pressure increases, the laminar burning velocity values are observed to decrease, and a maximum value of β is obtained at ϕ = 1.0 (T_u= 300 K) and 1.1 (T_u= 600 K). It is to be noted here that the values of pressure exponent β are negative. A maximum value of β indicates the least dependence on mixture pressure (or concentration of reactants within the combustion zone). Since the reactants are available optimally for stoichiometric and slightly rich mixtures, pressure exponent β has maximum values at these conditions. For extremely lean and rich mixture conditions, the mixture is either fuel or oxidizer deficient. Therefore, the deficiency of either fuel or oxidizer components in the mixture results in higher (negative) dependence on pressure (concentration of the reactants) within the combustion zone.

3.6. Pressure and temperature exponent variation

The current work suggests that the pressure exponent varies as a function of the temperature ratio and the temperature exponent as a function of the pressure ratio based on the detailed LBV measurements reported in the current work. A linear increment in the pressure and temperature exponent was noted for different mixture conditions (ϕ). Fig. 11 depicts the variation of the temperature and pressure exponents as a function of pressure ratio and temperature ratio, respectively, for selected mixture conditions (ϕ = 0.7, 1.0, and 1.3). The variation shows a linear dependency on each other. Fig. 11a exhibits the temperature exponent (α) variation at higher pressures for the stated mixture conditions (ϕ). The temperature exponent increases linearly with the pressure ratio. The pressure-dependent behavior of the temperature exponents shows a linear variation for stoichiometric mixtures [35]. The temperature exponent values are noted to increase with pressure, and the temperature exponent variation for the stoichiometric ethane-air mixture can be derived as α = 1.77 + 0.018 (P_u/P_{u0}). The temperature exponents are also compared with the reaction mechanism predictions of Aramco mech 1.3 [23]. The present measurements are reasonably closer to the kinetic model predictions at stoichiometric and rich mixture conditions. However, at lean mixture conditions, the kinetic model predictions are consistently higher than the current results, with a maximum deviation of ~ 4 % at P_u = 1 atm. Fig. 11b illustrates the pressure exponent (β) variation with temperature ratio for the stated mixture conditions (ϕ). It is evident from Fig. 11b that the mechanism predictions of Aramco mech 1.3 [23] are marginally higher than the current measurements for lean mixture conditions over the entire temperature range. However, they match well with the current results at stoichiometric and rich mixture conditions. A maximum deviation of ~ 11 % at reference temperature for stoichiometric mixture condition is noted. The slope of the linear fit curves of temperature exponent values (α) shown in Fig. 11a is significantly lower than the slopes of pressure exponents (β) values shown in Fig. 11b. This indicates that the pressure exponent values (β) are more temperature dependent than the dependence of temperature exponent values (α) on the pressure ratio. It is obvious from Fig. 11 that it is necessary to consider the pressure and temperature dependencies of temperature and pressure exponents (α, β), as compared to the constant (α, β) values reported by various researchers earlier [1,6,8,10,11] in the standard power-law correlations. Based on the current experimental observations, a revised power-law correlation is proposed by accounting for the variation of α and β as

$$S_u = S_{u0}\left(\frac{T_u}{T_{u0}}\right)^{\alpha_0+\alpha_1\left(1-\frac{P_u}{P_{u0}}\right)}\left(\frac{P_u}{P_{u0}}\right)^{\beta_0+\beta_1\left(1-\frac{T_u}{T_{u0}}\right)} \tag{5}$$

where α_i and β_i are the linear fit coefficients acquired from Fig. 11. For different equivalence ratios, the temperature/pressure exponent depends on the values of coefficients α_0 and α_1, and β_0 and β_1, respectively. The equivalence ratio plays a role in the temperature/pressure exponent variation, as shown in Figs. 7 and 10. All the linear fit coefficients, along with the LBV values (S_{u0}) at reference conditions (P_u = 1 atm, T_{u0} = 300 K) are listed in the attached supplementary material.

Lowry et al. [8] proposed the expression for LBV variation as a function of pressure and equivalence ratio. They ignored the effect of temperature because the study was carried out at 298 K. There are no other LBV expressions reporting the variation of the LBV of ethane-air mixtures at different operating conditions in the literature except Lowry et al. [8].

Lowry et al. [8]:

$$S_u = \left(-98.339 + 250.161\phi - 141.178\phi^2\right)(1/P_u)^{\left(1.161-1.79\phi+0.837\phi^2\right)}$$

Present work: $S_u = S_u(T_u/T_{uo})^{(\alpha_o+\alpha_1(1-P_u/P_{uo}))}(P_u/P_{uo})^{(\beta_o+\beta_1(1-T_u/T_{uo}))}$

In the present work, an inter-dependency between the temperature and pressure exponent was observed. From the detailed analysis of the present data, a linear correlation is observed for pressure ratio (P_u/P_{u0})

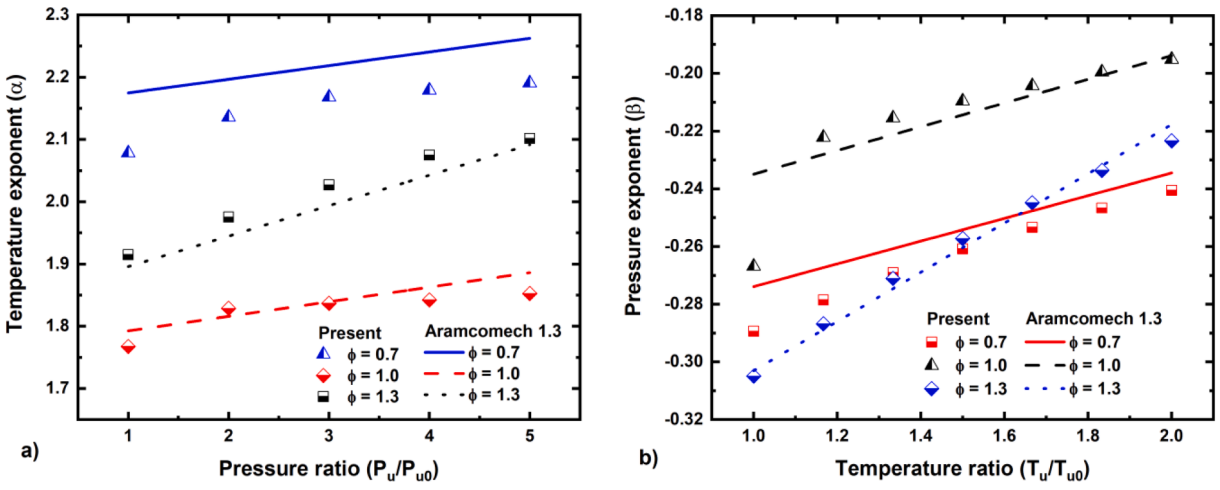

Fig. 11. (a) Temperature exponent (α) variation with pressure ratio and (b) Pressure exponent (β) variation with temperature ratios of an ethane-air mixture.

versus temperature exponent (α) (Fig. 11 (a)) and temperature ratio (T_u/T_{u0}) versus pressure exponent (β) (Fig. 11 (b)). Similar correlations were reported by Shinde et al. [22], and Varghese et al. [21] at high pressure and high temperature conditions. Several efforts were made to match the present data with other correlations reported in the literature [36]. However, none of the existing correlations were able to accurately represent the behavior of premixed hydrocarbon-air flames at high pressure and high temperature conditions. The correlation proposed in this work helped provide better insights on the flame propagation behavior. The variation of LBV at elevated pressure and temperature at stoichiometric mixture condition is shown in the supplementary material (Fig. S2).

3.7. Chemical kinetic analysis

3.7.1. Sensitivity analysis

Sensitivity coefficients help delineate the influence of different species and reactions on the variation of the LBV. It helps evaluate the significance of important major reactions, initial concentrations, boundary conditions, and their effect on combustion emissions and the development of optimized combustion models [37]. The sensitivity analysis results are very useful for refining the comprehensive kinetic models by modifying/removing the reactions or species with low sensitivity coefficients or adding new species/reactions that have a major effect on the LBV. The normalized sensitivity coefficient for the LBV is defined in Eq. (6) as the fractional change in the mixture burning velocity. S_{ui} caused by a fractional change in the rate of a specific reaction k_j [38].

$$\mathrm{Sens}\,(S_u,\,k) = \frac{\partial \log S_{ui}}{\partial \log k_j} = \frac{k_j}{S_{ui}}\left(\frac{\partial S_{ui}}{\partial k_j}\right) \tag{6}$$

where S_{ui} is the laminar burning velocity of species i and k_j is the reaction rate of reaction j.

The sensitivity analysis of the major reactions from the Aramco mech 1.3 [23] mechanism has been studied for the C_2H_6-air mixtures at various mixture strengths (ϕ = 0.7, 1.0, and 1.3), mixture temperatures

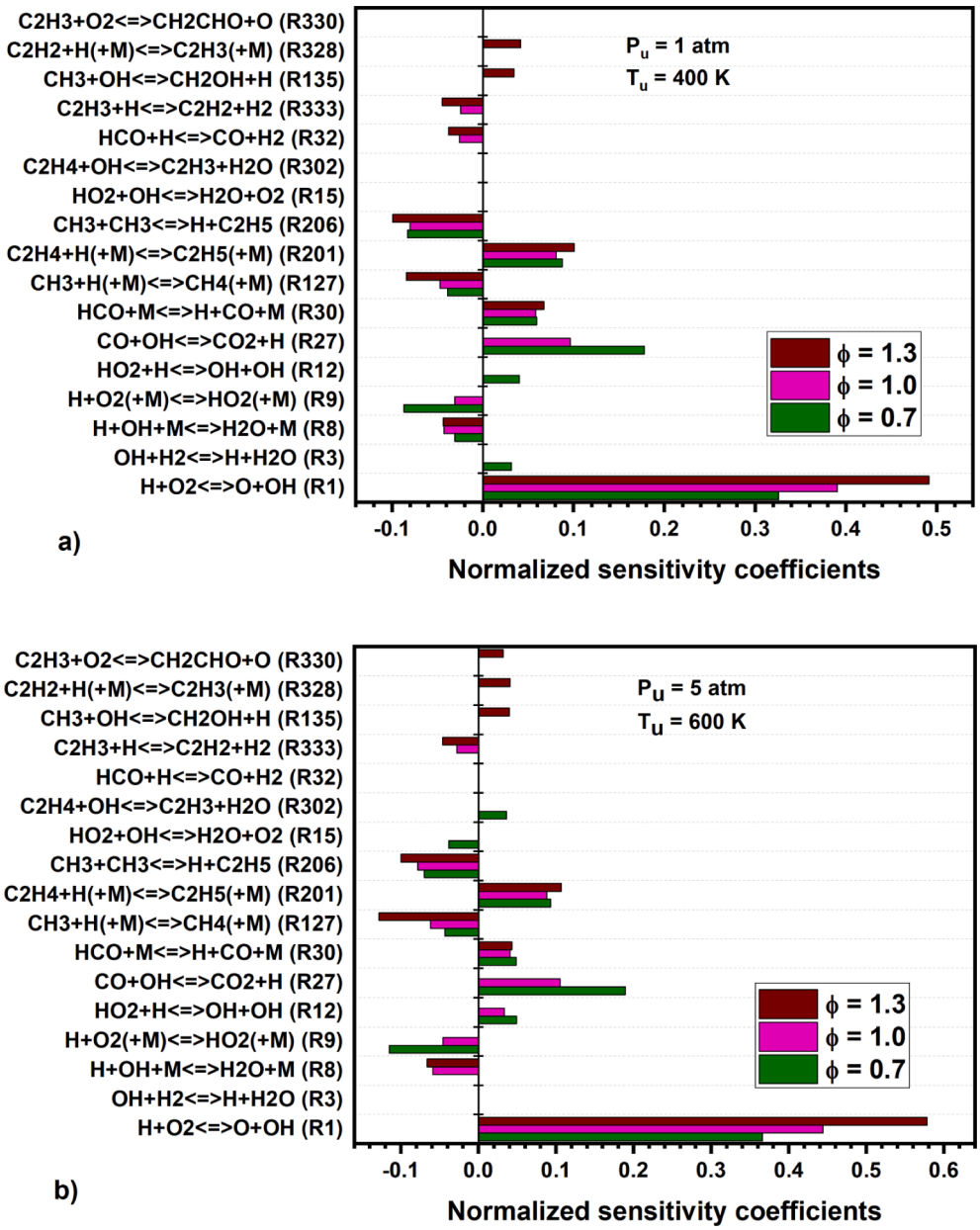

Fig. 12. Normalized sensitivity analysis of ethane-air mixture at (a) 400 K, 1 atm and (b) 600 K, 5 atm.

of 400 and 600 K, and mixture pressures of 1 and 5 atm.

Fig. 12a and 12b indicate the influence of 17 key elementary reactions out of a total of 1542 reactions on the LBV of C_2H_6-air mixtures at various mixture conditions of 1 atm 400 K, and 5 atm 600 K, respectively. The LBV increases due to elementary reactions with positive normalized sensitivity coefficient values and vice versa for elementary reactions with negative sensitivity coefficient values. At all mixture conditions, reactions featuring H radicals were the most highly sensitive, and their sensitivity enhanced with an increase in pressure and temperature. Due to the rise in pressure and temperature, the sensitivity coefficients of most of the elementary reactions increases, whereas some reactions become active and inactive owing to a rise in the overall reactivity and rate of the consumption of radicals. The chain branching reaction $H + O_2 \leftrightarrow O + OH$ (R1) exhibits the maximum positive sensitivity coefficient across all mixture conditions, pressure, and temperature. Approximately 15 % rise in sensitivity coefficient is observed at all mixture conditions (ϕ), due to a rise in pressure and temperature. The major CO oxidation reaction, $CO + OH \leftrightarrow CO_2 + H$ (R27), generates heat, and an H radical enhances the sensitivity coefficient of reaction R1 that, further increases the LBV. In addition to R27, the decomposition of formyl radical (HCO) via the reaction $HCO + M \leftrightarrow H + CO + M$ (R30) is a substantial source of H-atoms for premixed ethane-air mixtures. The reactions R27 and R201 indicate a marginal increase in the sensitivity coefficients due to enhanced pressure and temperature conditions. The reactions R302, R12, and R330 become active at $\phi = 0.7$, 1.0, and 1.3, respectively, whereas reactions R3 and R8 become inactive at $\phi = 0.7$, and R32 at $\phi = 1.0$, 1.3, owing to rise in the mixture pressure and temperature conditions. The chain branching reaction $HCO + M \leftrightarrow H + CO + M$ (R30) showed the maximum decrement in the positive sensitivity across all mixture conditions, owing to the rise in the third body effects along with pressure and temperature. The negative sensitivity of the chain termination reaction $CH_3 + H (+M) \leftrightarrow CH_4 (+M)$ (R127) enhances by nearly 52 % at rich mixture conditions ($\phi = 1.3$) conditions, owing to an increase in the recombination of H radical and third body effects with pressure and temperature increment from 1 atm, 400 K to 5 atm, 600 K.

3.7.2. Reaction path analysis

Reaction pathway analysis (RPA) is a useful tool for the reduction of the kinetic models by featuring the major and minor channels from the detailed mechanism. It further helps to investigate the reaction chain that exhibits how other species contribute to the production or consumption of a selected set of species under examination. The arrow color or thickness indicates the strength of the flux along the pathway. The values on the arrow depict the net elemental flux of the C atom, and the shown values were normalized against the maximum net elemental flux in the diagram.

The elemental flux of the C atom from species j to species k via reaction step i can be evaluated [39] utilizing the following Eqn (7).

$$C_{ijk} = \frac{n_{C,j} n_{C,k} kr_i}{N_{C,i}} \tag{7}$$

C_{ijk} indicates the elemental flux of C atom from species j to species k in reaction i at an instance in time t, ${}^{n}C_j$, and ${}^{n}C_k$ are the number of C atoms in species j and k respectively, k_{ri} is the reaction rate from species j to k for reaction i, and $N_{c,i}$ is the total number of C atoms in reaction i for both products and reactants. The total elemental flux C_{jk} from species j to k is obtained by summing all elemental fluxes of C atom from species j to k.

Reaction pathways are drawn using the Aramco mech [23] mechanism with the Cantera tool [40], which uses the Graphviz [41] tool to generate a dot file and reaction pathway diagram. The oxidation of ethane starts from the H-abstraction of C_2H_6 by H, O, and OH radicals, producing the ethyl radical (C_2H_5), as shown in Fig. S1 (included in the supplementary material). The detailed oxidation diagram of the ethane-

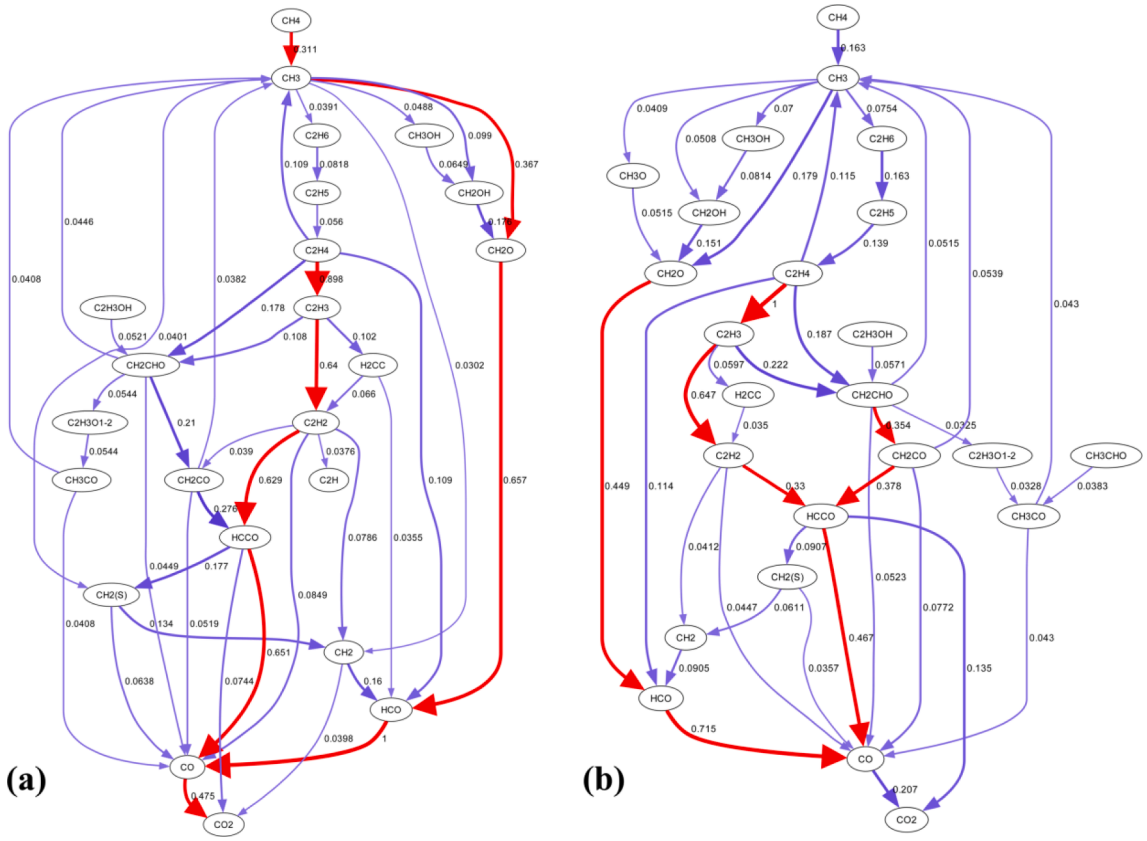

Fig. 13. Reaction pathway diagram of ethane-air mixture for the stoichiometric mixture condition at (a) 400 K, 1 atm and (b) 600 K, 5 atm.

air mixture at stoichiometric condition is included in the supplementary material. Fig. 13a and 13b show the reaction pathway diagram at stoichiometric mixture condition of ethane and air at mixture temperature and pressure of 400 K, 1 atm, and 600 K, 5 atm, respectively, for the reactor temperature of 1800 K. A threshold value of 3 % of the maximum net elemental flux was chosen and only species with values greater than this threshold were included in the diagram. Net elemental flux of values greater than 30 % of the maximum net elemental flux were highlighted in red color and were identified as major pathway.

The major reaction pathway for the mixture temperature of 400 K, and 1 atm pressure are as follows:

$$CH_4 \rightarrow CH_3 \rightarrow CH_2O \rightarrow HCO \rightarrow CO \rightarrow CO_2 \quad (8a)$$

$$C_2H_4 \rightarrow C_2H_3 \rightarrow C_2H_2 \rightarrow HCCO \rightarrow CO \rightarrow CO_2 \quad (8b)$$

Whereas the significant reaction pathways for the mixture temperature of 600 K and high pressure of 5 atm are as follows:

$$C_2H_4 \rightarrow C_2H_3 \rightarrow C_2H_2 \rightarrow HCCO \rightarrow CO \quad (9a)$$

$$CH_2CHO \rightarrow CH_2CO \rightarrow HCCO \rightarrow CO \quad (9b)$$

$$CH_2O \rightarrow HCO \rightarrow CO \quad (9c)$$

At high mixture temperature and pressure conditions (600 K, 5 atm), the reaction route $CH_2CHO \rightarrow CH_2CO$ exhibits higher elemental flux values than the threshold value and helps in the formation of ketyl radical, HCCO. The maximum net reduction in the elemental flux is observed for the reaction between the species carbon dioxide (CO_2) and carbon monoxide (CO) by 56 % through different reactions. The maximum increment in elemental flux is observed from 0.056 (at 400 K, 1 atm) to 0.139 (at 600 K, 5 atm) by ~ 150 % in the production of ethylene (C_2H_4) from ethyl radical (C_2H_5). The ethylene species is one of the prominent species in the major reaction pathway diagram (Eqn. (8b) and (9a). The change in elemental flux of various reactions can be seen in Fig. 13 (b) as compared to Fig. 13 (a) due to the simultaneous effect of pressure and temperature, and many reactions exhibit net elemental flux values lower/higher than the threshold values resulting in the absence/presence in the pathway diagrams.

4. Conclusions

The EHDC method is utilized to evaluate the LBV of ethane-air mixtures for a range of mixture strength (ϕ = 0.7-1.3) at high temperature (350-620 K) and high pressure (1-5 atm) conditions. The external heating minimizes the heat loss from the channel walls and helps to obtain nearly adiabatic, stabilized planar flames (due to the high aspect ratio of the channel) to measure the LBV at given conditions. The temperature and pressure exponents are evaluated from the burning velocity measurements. The present LBV measurements are in a better match with the existing measurements in the literature. The specific outcomes of the present investigation are summarized as follows.

- The LBV is noted to enhance with the unburnt mixture temperature and decreases with pressure for all mixture strength (ϕ). The variation of LBV measurement follows a parabolic curve with the mixture strength (ϕ), along with the maximum at $\phi = 1.1$.
- The reaction mechanism predictions of Aramco mech 1.3 [23] show a better match with the current results for the majority of mixture temperature, pressure, and equivalence ratio conditions (ϕ).
- The temperature exponent values (α) follow an inverted parabolic trend with the mixture conditions (ϕ), with a minimum at $\phi = 1.1$. The variation of pressure exponent (β) with the mixture conditions (ϕ) is similar to the LBV, along with maxima at $\phi = 1.0$.
- The temperature exponent (α) and pressure exponent (β) increases linearly with the pressure ratio and temperature ratio, respectively, for the entire range of mixture conditions (ϕ).
- The present work recommends a revised power-law correlation, indicating different behavior of temperature and pressure exponents as: $S_u = S_{u0}(T_u/T_{u0})^{\alpha_0 + \alpha_1(1 - P_u/P_{u0})}(P_u/P_{u0})^{\beta_0 + \beta_1(1 - T_u/T_{u0})}$.
- The maximum decrement in positive sensitivity was observed for the chain branching reaction HCO + M ↔ H + CO + M (R30) across all mixture conditions, owing to the rise in the third body effects along with pressure and temperature. However, the negative sensitivity of the chain termination reaction CH_3 + H (+M) ↔ CH_4 (+M) (R127) enhances by nearly 52 % at rich mixture ($\phi = 1.3$) conditions, owing to an increase in the recombination of H radical and third body effects with a pressure and temperature increment from 1 atm, 400 K to 5 atm, 600 K.
- The reaction pathway analysis observes a maximum net reduction in the elemental flux for the reaction between the species carbon dioxide (CO_2) and carbon monoxide (CO) by 56 % through different reactions due to a rise in pressure and temperature. The maximum increment in elemental flux is noted from 0.056 (at 400 K, 1 atm) to 0.139 (at 600 K, 5 atm) by ~ 150 % in the production of ethylene (C_2H_4) from ethyl radical (C_2H_5).

Declaration of Competing Interest

The authors declare that they have no known competing financial interests or personal relationships that could have appeared to influence the work reported in this paper.

Data availability

Data will be made available on request.

Acknowledgement

The Science and Engineering Research Board of India, SERB, funded this research (Project number CRG/2020/001700). The corresponding author, Vijay Shinde is grateful to his parent institute K. J. Somaiya College of Engineering, Mumbai, for sponsoring to pursue a doctoral program at IIT Bombay, and also to Mr. Jitendra Kumar for his sincere support and assistance during experimental measurements.

Appendix A. Supplementary data

Supplementary data to this article can be found online at https://doi.org/10.1016/j.fuel.2023.130175.

References

[1] Hassan MI, Aung KT, Kwon OC, Faeth GM. Properties of laminar premixed hydrocarbon/air flames at various pressures. J Propul Power 1998;14:479–88. https://doi.org/10.2514/2.5304.
[2] Egolfopoulos FN, Zhu DL, Law CK. Experimental and numerical determination of laminar flame speeds: Mixtures of C_2-hydrocarbons with oxygen and nitrogen. Symp Combust 1991;23:471–8. https://doi.org/10.1016/S0082-0784(06)80293-6.
[3] Konnov AA, Dyakov IV, De Ruyck J. Measurement of adiabatic burning velocity in ethane-oxygen-nitrogen and in ethane-oxygen-argon mixtures. Exp Therm Fluid Sci 2003;27:379–84. https://doi.org/10.1016/S0894-1777(02)00242-X.
[4] Tseng LK, Ismail MA, Faeth GM. Laminar burning velocities and Markstein numbers of hydrocarbon air flames. Combust Flame 1993;95:410–26. https://doi.org/10.1016/0010-2180(93)90007-P.
[5] Aung KT, Tseng LK, Ismail MA, Faeth GM. Response to comment by S.C. Taylor and D.B. Smith on "laminar burning velocities and Markstein numbers of hydrocarbon/air flames". Combust Flame 1995;102:526–30. https://doi.org/10.1016/0010-2180(95)00035-5.
[6] Jomaas G, Zheng XL, Zhu DL, Law CK. Experimental determination of counterflow ignition temperatures and laminar flame speeds of C2–C3 hydrocarbons at atmospheric and elevated pressures. Proc Combust Inst 2005;30:193–200. https://doi.org/10.1016/j.proci.2004.08.228.
[7] Ratna Kishore V, Duhan N, Ravi MR, Ray A. Measurement of adiabatic burning velocity in natural gas-like mixtures. Exp Therm Fluid Sci 2008;33:10–6. https://doi.org/10.1016/j.expthermflusci.2008.06.001.
[8] Lowry W, De Vries J, Krejci M, Petersen E, Serinyel Z, Metcalfe W, et al. Laminar flame speed measurements and modeling of pure alkanes and alkane blends at

elevated pressures. J Eng Gas Turbines Power 2011;133:1–9. https://doi.org/10.1115/1.4002809.
[9] Mitu M, Razus D, Giurcan V, Oancea D. Experimental and numerical study of laminar burning velocity of ethane–air mixtures of variable initial composition, temperature and pressure. Energy Fuel 2014;28:2179–88.
[10] Mitu M, Razus D, Giurcan V, Oancea D. Normal burning velocity and propagation speed of ethane-air: Pressure and temperature dependence. Fuel 2015;147:27–34. https://doi.org/10.1016/j.fuel.2015.01.026.
[11] Goswami M, Bastiaans RJM, De Goey LPH, Konnov AA. Experimental and modelling study of the effect of elevated pressure on ethane and propane flames. Fuel 2016;166:410–8. https://doi.org/10.1016/j.fuel.2015.11.013.
[12] Han X, Wang Z, Wang S, Whiddon R, He Y, Lv Y, et al. Parametrization of the temperature dependence of laminar burning velocity for methane and ethane flames. Fuel 2019;239:1028–37. https://doi.org/10.1016/j.fuel.2018.11.118.
[13] Shinde V, Fulzele A, Kumar S. Laminar burning velocity measurements of C1–C4 alkane-air mixtures at elevated mixture temperatures. Fuel 2023;352:129096. https://doi.org/10.1016/j.fuel.2023.129096.
[14] Gu XJ, Haq MZ, Lawes M, Woolley R. Laminar burning velocity and Markstein lengths of methane-air mixtures. Combust Flame 2000;121:41–58. https://doi.org/10.1016/S0010-2180(99)00142-X.
[15] Vagelopoulos CM, Egolfopoulos FN. Direct experimental determination of laminar flame speeds. Symp Combust 1998;27:513–9. https://doi.org/10.1016/S0082-0784(98)80441-4.
[16] Bosschaart KJ, De Goey LPH. The laminar burning velocity of flames propagating in mixtures of hydrocarbons and air measured with the heat flux method. Combust Flame 2004;136:261–9. https://doi.org/10.1016/j.combustflame.2003.10.005.
[17] Dyakov IV, De Ruyck J, Konnov AA. Probe sampling measurements and modeling of nitric oxide formation in ethane + air flames. Fuel 2007;86:98–105. https://doi.org/10.1016/j.fuel.2006.06.003.
[18] Dirrenberger P, Le Gall H, Bounaceur R, Herbinet O, Glaude PA, Konnov A, et al. Measurements of laminar flame velocity for components of natural gas. Energy Fuel 2011;25:3875–84. https://doi.org/10.1021/ef200707h.
[19] Park O, Veloo PS, Egolfopoulos FN. Flame studies of C_2 hydrocarbons. Proc Combust Inst 2013;34:711–8. https://doi.org/10.1016/j.proci.2012.06.159.
[20] Ghosh A, Munoz-Munoz NM, Chatelain KP, Lacoste DA. Laminar burning velocity of hydrogen, methane, ethane, ethylene, and propane flames at near-cryogenic temperatures. Appl Energy Combust Sci 2022;12:100094. https://doi.org/10.1016/j.jaecs.2022.100094.
[21] Varghese RJ, Kolekar H, Kishore VR, Kumar S. Measurement of laminar burning velocities of methane-air mixtures simultaneously at elevated pressures and elevated temperatures. Fuel 2019:257. https://doi.org/10.1016/j.fuel.2019.116120.
[22] Shinde V, Fulzele A, Kumar S. Experimental measurements of laminar burning velocity of premixed propane-air flames at higher pressure and temperature conditions. Fuel 2024;356:129561. https://doi.org/10.1016/j.fuel.2023.129561.
[23] Metcalfe WK, Burke SM, Ahmed SS, Curran HJ. A hierarchical and comparative kinetic modeling study of C1–C2 hydrocarbon and oxygenated fuels. Int J Chem Kinet 2013;45:638–75. https://doi.org/10.1002/kin.20802.
[24] H. Wang X. You A.V. Joshi SG. Davis A. Laskin F. Egolfopoulos et al. High-temperature combustion reaction model of H_2. High-Temperature Combust React Model H_2/CO/C_1-C_4 Compd 2007.
[25] F. Williams Chemical-kinetic mechanisms for combustion applications. San Diego Mechanism web page, Mechanical and Aerospace Engineering (Combustion Research), at San Diego.(2018) 2014.
[26] Varghese RJ, Kolekar H, Hariharan V, Kumar S. Effect of CO content on laminar burning velocities of syngas-air premixed flames at elevated temperatures. Fuel 2018;214:144–53. https://doi.org/10.1016/j.fuel.2017.10.131.
[27] Maruta K, Kataoka T, Kim N, Minaev S, Fursenko R. Characteristics of combustion in a narrow channel with a temperature gradient. Proc Combust Inst 2005;30 II: 2429–36. https://doi.org/10.1016/j.proci.2004.08.245.
[28] Kumar S, Maruta K, Minaev S, Fursenko R. Appearance of target pattern and spiral flames in radial microchannels with CH_4-air mixtures. Phys Fluids 2008:20. https://doi.org/10.1063/1.2836670.
[29] Varghese RJ, Kolekar H, Kumar S. Laminar burning velocities of H_2/CO/CH_4/CO_2/N_2 -air mixtures at elevated temperatures. Int J Hydrogen Energy 2019;44: 12188–99. https://doi.org/10.1016/j.ijhydene.2019.03.103.
[30] Varghese RJ, Kolekar H, Kumar S. Demarcation of reaction effects on laminar burning velocities of diluted syngas–air mixtures at elevated temperatures. Int J Chem Kinet 2019;51:95–104. https://doi.org/10.1002/kin.21232.
[31] Alekseev VA, Christensen M, Konnov AA. The effect of temperature on the adiabatic burning velocities of diluted hydrogen flames: A kinetic study using an updated mechanism. Combust Flame 2015;162:1884–98. https://doi.org/10.1016/j.combustflame.2014.12.009.
[32] RJ. Kee FM. Rupley Miller JA. Chemkin-II 1989 A Fortran chemical kinetics package for the analysis of gas-phase chemical kinetics. Sandia National Lab.(SNL-CA) Livermore CA (United States) 10.2172/5681118.
[33] Kuo KK. Principles of combustion. second ed. New Jersey: John Wiley & Sons, Inc.; 2005.
[34] Konnov AA. The temperature and pressure dependences of the laminar burning velocity: experiments and modelling. Hungary: Proc. Eur. Combust. Meet. Budapest; 2015.
[35] Han P, David Checkel M, Fleck BA, Nowicki NL. Burning velocity of methane/diluent mixture with reformer gas addition. Fuel 2007;86:585–96. https://doi.org/10.1016/j.fuel.2006.08.011.
[36] Wang Y, Movaghar A, Wang Z, Liu Z, Sun W, Egolfopoulos FN, et al. Laminar flame speeds of methane/air mixtures at engine conditions: Performance of different kinetic models and power-law correlations. Combust Flame 2020;218:101–8. https://doi.org/10.1016/j.combustflame.2020.05.004.
[37] Dunker AM. The decoupled direct method for calculating sensitivity coefficients in chemical kinetics. J Chem Phys 1984;81:2385–93. https://doi.org/10.1063/1.447938.
[38] Turányi T. Applications of sensitivity analysis to combustion chemistry. Reliab Eng Syst Saf 1997;57:41–8. https://doi.org/10.1016/S0951-8320(97)00016-1.
[39] Turányi T, Tomlin AS. Analysis of kinetic reaction mechanisms 2014;vol. 20. https://doi.org/10.1007/978-3-662-44562-4.
[40] DG. Goodwin HK. Moffat RL. Speth Cantera: An object-oriented software toolkit for chemical kinetics, thermodynamics, and transport processes 2018.
[41] Ellson J, Gansner E, Koutsofios L, North SC, Woodhull G. Graphviz—Open source graph drawing tools. Graph Draw. 9th Int. Symp. GD, Vienna, Austria, Sept. 23–26, 2001 Revis. Pap. 9. Springer 2001;2002:483–4. https://doi.org/10.1007/3-540-45848-4_57.